frontiers | Frontiers in Environmental Science

TYPE Original Research
PUBLISHED 21 June 2023
DOI 10.3389/fenvs.2023.1186147

OPEN ACCESS

EDITED BY
Delong Meng,
Central South University, China

REVIEWED BY
Jun Chen,
Anhui University of Science and Technology, China
Sudipta Rakshit,
Tennessee State University, United States

*CORRESPONDENCE
Zijia Zhang,
zhangzijia6814@gmail.com
Xiheng Hu,
huxiheng@csu.edu.cn

RECEIVED 14 March 2023
ACCEPTED 02 June 2023
PUBLISHED 21 June 2023

CITATION
Liu X, Xue W, Zhang Z, Zhou W, Song S, Li Y, Benzaazoua M and Hu X (2023), Effect of cobalt isomorphic substitution on the properties of goethite and the adsorption of lead.
Front. Environ. Sci. 11:1186147.
doi: 10.3389/fenvs.2023.1186147

Effect of cobalt isomorphic substitution on the properties of goethite and the adsorption of lead

Xu Liu[1,2,3], Wenlu Xue[1,2], Zijia Zhang[1,2,4]*, Wei Zhou[5], Shaoxian Song[1,2], Yinta Li[6], Mostafa Benzaazoua[7] and Xiheng Hu[8,9,10,11,12,13]*

[1]Hubei Key Laboratory of Mineral Resources Processing and Environment, Wuhan University of Technology, Wuhan, Hubei, China, [2]School of Resources and Environmental Engineering, Wuhan University of Technology, Wuhan, Hubei, China, [3]Jinan Municipal Engineering Design Group, Jinan, Shandong, China, [4]Doctorado Institucional en Ingeniería y Ciencia de Materiales, Universidad Autonoma San Luis Potosi, San Luis Potosi, Mexico, [5]School of Science, Wuhan University of Technology, Wuhan, Hubei, China, [6]Department of Food Engineering, Weihai Ocean Vocational College, Weihai, Shandong, China, [7]Mohammed VI Polytechnic University (UM6P), Geology and Sustainable Mining, Ben Guerir, Morocco, [8]Department of Urology, Xiangya Hospital, Central South University, Changsha, China, [9]The Department of Dermatology, Xiangya Hospital, Central South University, Changsha, China, [10]National Engineering Research Center of Personalized Diagnostic and Therapeutic Technology, Changsha, China, [11]Furong Laboratory, Changsha, Hunan, China, [12]Hunan Key Laboratory of Skin Cancer and Psoriasis, Hunan Engineering Research Center of Skin Health and Disease, Xiangya Hospital, Changsha, China, [13]National Clinical Research Center for Geriatric Disorders, Xiangya Hospital, Changsha, China

Iron oxides are ubiquitous in the environment and often contain impurities because of their substitution by Al, Mn, Co, and other metals. However, few studies have focused on Co substitution and subsequent Pb(II) adsorption on its surfaces. Herein, the effect of the isomorphic substitution of Co on the physiochemical properties of goethite and the atomic-level mechanisms of lead sorption in relation to structural changes were investigated in this work. The results showed that Co substitution reduced the unit cell parameters and crystallinity of goethite. More Fe-OH groups on the surface were exposed with Co substitution, leading to the preferential sorption of Pb. The DFT calculations further revealed that the valence band was shortened and the total density of states was more biased towards the Fermi level in Co-substituted goethite, making the surface electrons more active. In addition, both Pb^{2+} and $Pb(OH)^{+}$ were adsorbed by goethite, forming a tridentate complex with three oxygen atoms. In this process, sp3 hybridization mainly occurred. These results provide a new perspective for studying the properties of Co-substituted goethite and its reaction with lead, helping to expand the application of DFT calculations to simulate and predict the fixation and mobilization of heavy metals in goethite-rich soils/sediments.

KEYWORDS

goethite, cobalt, isomorphous substitution, DFT, adsorption of lead

1 Introduction

Goethite (α-FeOOH) is one of the most common and important crystalline iron oxide minerals in the soil and plays a significant role in the retention and transformation of heavy metals such as Pb(II), Ni(II), Co(II), and Mn(II) (Jackson, 2005). Nevertheless, because of the structural characteristics like heteroatomic isomorphism caused by atomic vacancies and defects, goethite is unlikely to exist in its pure form, and elements, such as Al, Mn, Cr, Co,

and Ni, may exist in its structure (Kühnel, 1975; Norrish, 1975). Among them, cobalt, as a strategic metal, is widely used in the electronics industry and the new energy vehicle industry (Huang et al., 2020). With the rapid development of these industries, the demand for cobalt continues to increase, which also leads to more and more cobalt entering the environment, greatly increasing the possibility of cobalt isomorphic substitution goethite.

Previous studies have shown that goethite with isomorphic substitutions have a significant change in mineral characteristics and adsorption properties. For example, the substitution of aluminum in goethite crystals affected not only the distance between adjacent crystal planes but also the structural arrangement of iron atoms, electron orbital hybridization, and charge transfer, thus realizing the preferential adsorption of phosphate (Hsu et al., 2020). The introduction of manganese increased the surface roughness of goethite and improved the adsorption capacity of goethite for uranium (Zhang et al., 2020). Cobalt has been used to substitute goethite to prepare magnetic particle precursors (Iwasaki and Yamamura, 2002), and obtained a faster dissolution rate (Alvarez et al., 2008). However, current research on cobalt isomorphic substitution goethite has focused on the changes in crystal structure after the substitution, with little attention paid to the impact of substitution on the adsorption performance and mechanisms of heavy metals (Cornell et al., 1996; Gasser et al., 1996). In this case, it is of great significance to further study the adsorption properties of cobalt-substituted goethite and the mechanisms of interaction with heavy metals.

Density functional theory (DFT) has been proven to be a successful method for the study of the electronic structure of multi-electron systems, which is widely used in physics, chemistry, material science, and other fields, shifting the research perspective from the macroscopic to the atomic scale (Ding et al., 2014; Liu et al., 2016; Song et al., 2016; Hüffer et al., 2017). At present, it has also been fully explored in the research of geometric structure, energy, charge density distribution, and other related calculations, especially for the simulation of adsorption properties. For example, Yi et al. explored the Hg^{2+} adsorption and surface oxidation on the MoS_2 surface through DFT calculations (Yi et al., 2019). Hsu et al. determined a new insight into the PO_4 sorption and related structural properties of Al-substituted goethite (Hsu et al., 2020). Similarly, Kubicki et al. used DFT to study the structure, energies, and adsorption mechanism of Fe(II) onto the (010) face of goethite (Kubicki et al., 2017). However, there is almost no research on the Co isomorphic substitution and Pb(II) adsorption of goethite using DFT calculations.

In this work, goethite with different amounts of cobalt substitution were synthesized using the precipitation method and the physiochemical properties of samples were characterized by XRD, SEM, BET, XPS, and FT-IR. Meanwhile, DFT calculations were used to explore the crystal structure, surface properties, and adsorption mechanism of heavy metal Pb(II) on goethite from the atomic level.

2 Materials and methods

2.1 Reagents

All reagents used, including ferric nitrate nonahydrate ($Fe(NO_3)_3{\cdot}9H_2O$), cobalt nitrate hexahydrate ($Co(NO_3)_2{\cdot}6H_2O$), and sodium hydroxide (NaOH), were purchased from the Sinopharm Chemical Reagent Company, China, and were all of analytical grade. The ultrapure water produced by Milli-Q of 18.25 mΩ was boiled to ensure the presence of the minimum amount of CO_2.

2.2 Preparation of goethite and Co-substituted goethite

In this study, an improved method was used to synthesize the goethite according to the reported procedure of Geen et al. (van Geen et al., 1994). First, (0.5-x) mol $Fe(NO_3)_3{\cdot}9H_2O$ and x mol $Co(NO_3)_2{\cdot}6H_2O$ (x = 0.025, 0.05, 0.1) were dissolved in 1 L deionized water. Subsequently, 2.5 mol/L NaOH solution was added to the above solution at a rate of 50 mL/min until pH reached 12.00 ± 0.05. This solution was stirred for 30 min at 400 rpm using a mechanical stirrer, and the suspensions obtained were aged in the dryer at 60°C for 12 days. Finally, the suspended solids were centrifuged at 5,000 rpm and washed with Milli-Q deionized water until the conductivity was under 2 μS/cm. After being freeze-dried, the samples were stored in polypropylene containers in a closed desiccator. In addition, the samples were labeled as Co-G-0, Co-G-5, Co-G-10, and Co-G-20, according to the proportion of cobalt content before the reaction, respectively.

2.3 Analytical methods

The main mineral phase composition of goethite was determined by X-ray diffraction (XRD-Empyrean, Panalytical, Netherlands), and the XRD Rietveld structure refinement of goethite was conducted using TOPAS software. The specific surface area (SSA), pore volume, and pore size of samples were measured by N_2 adsorption-desorption using the Brunauer-Emmett-Teller (BET) method. The morphologic features of goethite were observed using a scanning electron microscope (SEM-JSM 7100F, Joel, Japan). X-ray photoelectron spectroscopy analysis was carried out on an ESCALAB 250Xi and all binding energies were at the neutral carbon peak at 284.8 eV. The Zeta potential of adsorbents was also obtained using a Zetasizer Nano ZS90 (Malvern Instruments, UK) to detect the stability of the system. Furthermore, the Fourier-transform infrared spectra (FT-IR-Nicolet 6700-Thermo Electron Scientific Instruments, United States) was used to characterize the functional groups of absorbents.

2.4 Computational methods

The computation was performed using all-electron density functional calculations implemented in the Dmol3 module (Yu et al., 2015). Considering the higher accuracy and better optimization results in describing the hydrogen bond (Ireta et al., 2004), the Perdew-Burke-Ernzerhof (PBE) generalized gradient approximation (GGA) was adopted in this study. At the same time, DFT + U was used to correct the dispersion force,

eliminating the influence of the van der Waals force. Self-consistent field (SCF) convergence was set to 2.0×10^{-5} eV/atom and Broyden-Fletcher-Goldfarb-Shanno (BFGS) was used to optimize the crystal structure until the maximum internal stress, force, and displacement between atoms converged to 0.2 GPa, 0.05 eV/Å, and 5×10^{-4} nm, respectively. The ultra-soft pseudopotential was used for calculation. The sampling density of k-points was described by Monkhorst-Pack and the Brillouin zone was $(2 \times 2 \times 1)$.

After the geometrical optimization, the adsorption energy and density of states were calculated. The feasibilities of the adsorption of Pb^{2+} and $Pb(OH)^{+}$ on the surface of goethite can be evaluated by the adsorption energies (Eads), which are defined as the energy difference between the reaction products and the reactants.

$$E_{ads} = E_{M-Goethite} - (E_M + E_{Goethite}) \quad (1)$$

where $E_{M-Goethite}$ represents the total energy of the adsorbed molecules (Pb^{2+} or $Pb(OH)^{+}$) and the goethite substrate. E_M and $E_{Goethite}$ are the energies of the adsorbed molecules and the goethite substrate, respectively.

3 Results and discussion

3.1 Characterization of the samples

3.1.1 XRD patterns of goethite samples

The X-ray diffraction spectra of samples are presented in Figure 1. The patterns corresponded quite well with that of the standard card of goethite (JCPDS 29-0713), confirming that pure goethite samples were synthesized. It can be clearly seen from Figure 1A that, as the content of Co in samples increased, the intensity of the diffraction peak decreased gradually, especially in the

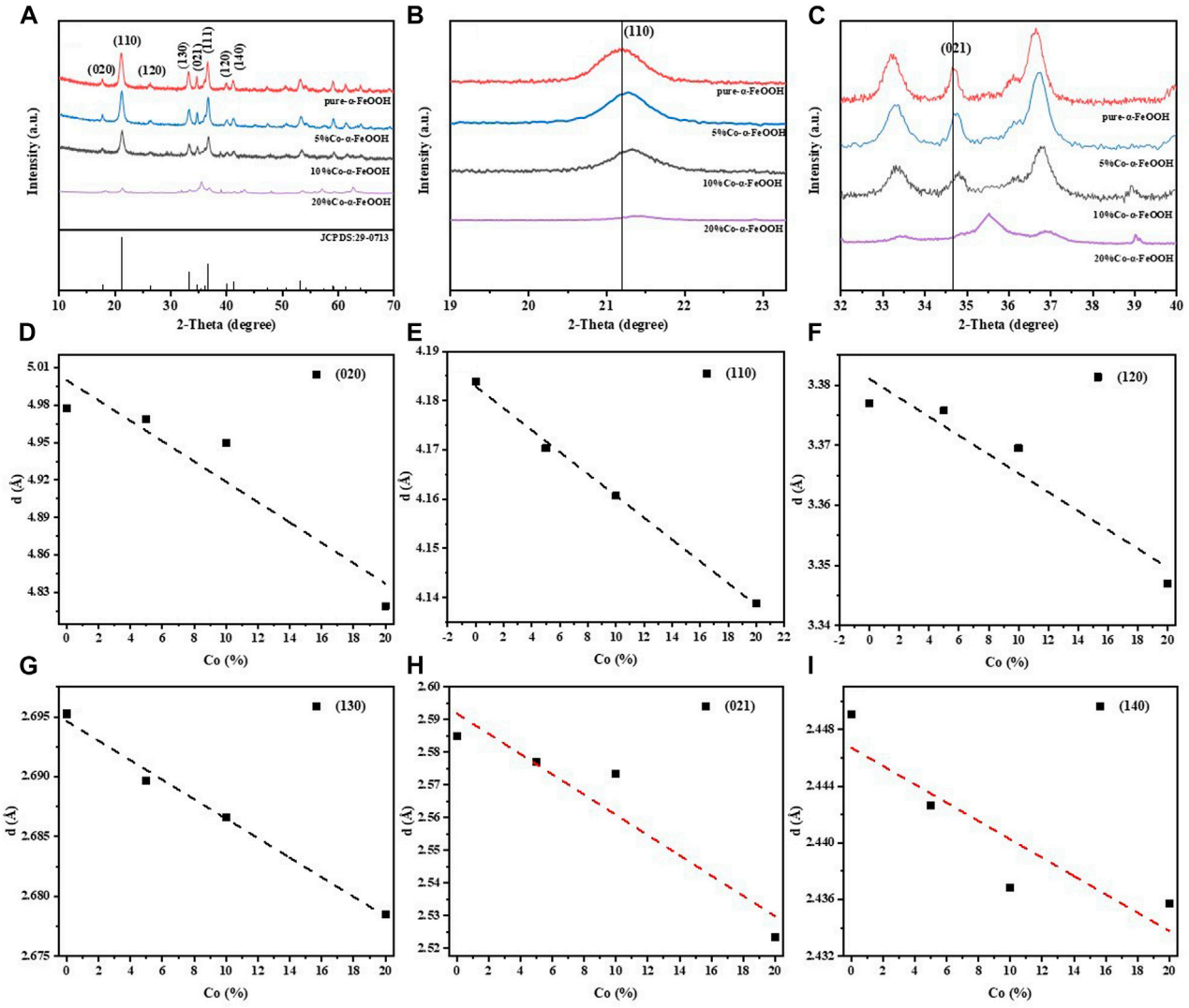

FIGURE 1
XRD patterns of samples: **(A)** the full spectrum of pure goethite and Co-substituted goethite samples (λ = 1.2438 Å), **(B)** XRD patterns of region near the (110) crystal plane in a 2-theta range of 19–23.5°and **(C)** XRD patterns of region near the (021) crystal plane in a 2-theta range of 32°–40°. The d value for individual planes of Co-substituted goethite **(D–I)**.

TABLE 1 Chemical compositions and their refined unit cell parameters.

Samples	G-Co-0	G-Co-5	G-Co-10	G-Co-20
Co contents (mol%)	0.00	5.39	9.36	19.00
△Co contents (mol%)	0.00	0.39	−0.64	−1.00
a (Å)	4.615238	4.605927	4.601953	4.604453
b (Å)	9.958332	9.946575	9.931874	9.893089
c (Å)	3.023158	3.021358	3.01366	2.992669
volume (Å3)	138.9446	138.4181	137.7424	136.3228
CrySize (nm)	20.2	18.3	17.6	16.7
Rwp (%)	10.17	9.3	7.48	7.17

peaks of (110) and (021). Some characteristic peaks disappeared along with some miscellaneous peaks emerging when the Co isomorphic substitution amount increased to 20%. At the same time, the addition of Co shifted the (110) and (021) crystal planes of goethite to the right; the higher the content of Co, the more obvious the shift. In addition, in Figures 1D–I, it can be seen that the d-spacing between the crystal planes of goethite gradually decreased with the increase of Co content. These results suggested that the introduction of Co into the octahedral interlayer structures caused a certain change in the crystal planes (Shannon, 1976; Schwertmann et al., 1977).

Based on the standard goethite crystal model (JCPDS: 29-0713), the Rietveld structure refinement of these Co-substituted goethite samples was conducted using TOPAS software. The results of the structural refinements and elemental analysis are listed in Table 1, from which it can be seen that with the increasing Co content, the unit cell parameters b and c were gradually reduced from 9.958 Å to 9.893 Å and from 3.023 Å to 2.992 Å, respectively. Meanwhile, the cell volume decreased from 138.94 $Å^3$ to 136.32 $Å^3$. The phenomenon that the crystal cells were all decreasing can be observed in Al-, Cr-, and Co-substituted goethite samples due to their smaller radius compared with Fe ions (Sileo et al., 2004; Alvarez et al., 2008; Liu et al., 2013; HuanLiu et al., 2018). Additionally, as the amount of Co applied in the process of preparing Co-substituted goethite increased, the amount of Co isomorphic substitution also increased, while △Co mol% (actual content - preliminary content) presented the phenomenon of gradually increasing from 0.00 mol% to 0.39 mol% and then decreasing to −1.00 mol%, indicating that a low content of Co can allow more Co to enter the goethite structure to form isomorphic substitutions.

3.1.2 SEM images and surface properties of goethite samples

Figure 2 showed the SEM images of the 0 mol% and 10 mol% Co-substituted goethite samples. Through the statistics of the particle size, the average length of the non-substitutional goethite was 261 nm, the width was 29 nm, and the aspect ratio was 9. But for 10 mol% Co-substituted goethite, the average length and width were 234 nm and 29 nm, respectively. The aspect ratio was about 8.06, which indicated that the length of goethite can be obviously shortened by Co isomorphic substitution. Moreover, the degree of crystallinity of Co-substituted goethite was significantly different from that of non-substitutional goethite. It can be found that the pure goethite had a better degree of crystallinity, and the planes and structure of goethite were relatively smooth and complete, while the Co-substituted goethite had a poorer degree of crystallinity with a great length difference and uneven crystal planes, which further illustrated the conclusion of XRD and was consistent with the results measured by Liang et al. (2021).

The surface charge of minerals can have an impact on the properties. It can be seen from Figure 3 that, as the pH increased, the surface charge of goethite decreased gradually (Liang et al., 2021). Furthermore, the zero charge point (pH_{pzc}) of goethite decreased with the increasing of Co content, indicating that goethite with a large Co isomorphic substitution was more likely to exhibit a deprotonation state and had a stronger surface electronegativity under the same pH conditions, which can have a positive effect on the adsorption of cations on the goethite surface.

The specific surface area analysis results are shown in Figure 4 and Table 2, from which it can be seen that the isomorphic substitution content of Co had a great impact on the specific surface area and pore diameter of goethite. In terms of pore size, all goethite samples were mainly micropores which were less than 2 nm and basically between 2 and 500 Å. It was worth noting that the micropores of goethite around 25 Å, which occupied a dominant

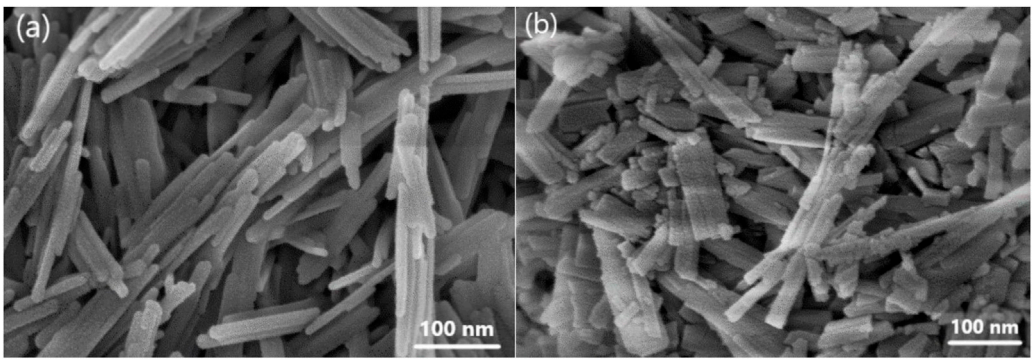

FIGURE 2
SEM images of goethite samples with **(A)** 0 mol% and **(B)** 10 mol% Co isomorphic substitution.

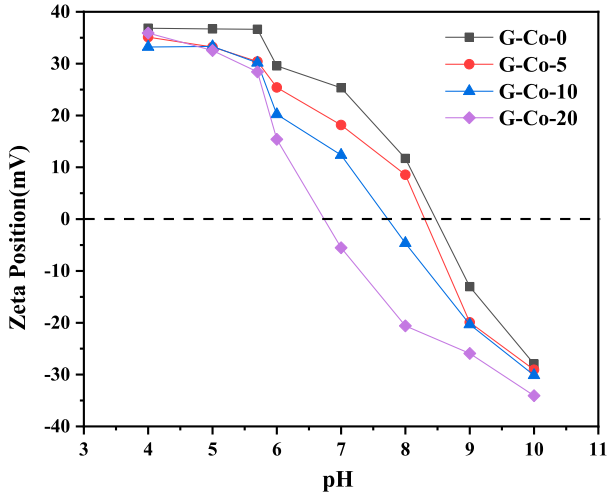

FIGURE 3
Zeta potential of pure goethite and Co isomorphic substituted goethite.

position in pore size of all samples, were almost unaffected by the isomorphic substitution of Co, while the number of micropores that had a diameter of about 300 Å was significantly reduced with the increasing content of Co. The results illustrated that it was micropores with larger diameters in goethite that were more easily be affected by Co isomorphic substitution. As is well known, BET is influenced by both grain size and pore structure, with smaller grain size and more pores resulting in larger specific surface area. Combining XRD (Figure 1) and pore structure (Table 2), it can be seen that, as the amount of Co isomorphic substitution gradually increases, the grain size gradually decreases while the larger diameter micropores gradually decrease. This is the main reason why the BET of goethite increases first and then decreases with the increase of Co isomorphic substitution.

3.1.3 XPS and FT-IR spectra of goethite samples

To better investigate the structural information such as the element existence state and chemical groups of the sample surface, X-ray photoelectron spectroscopy (XPS) and Fourier-transform infrared spectroscopies (FT-IR) were used and the results are shown in Figure 5. After fitting the XPS curve of Fe

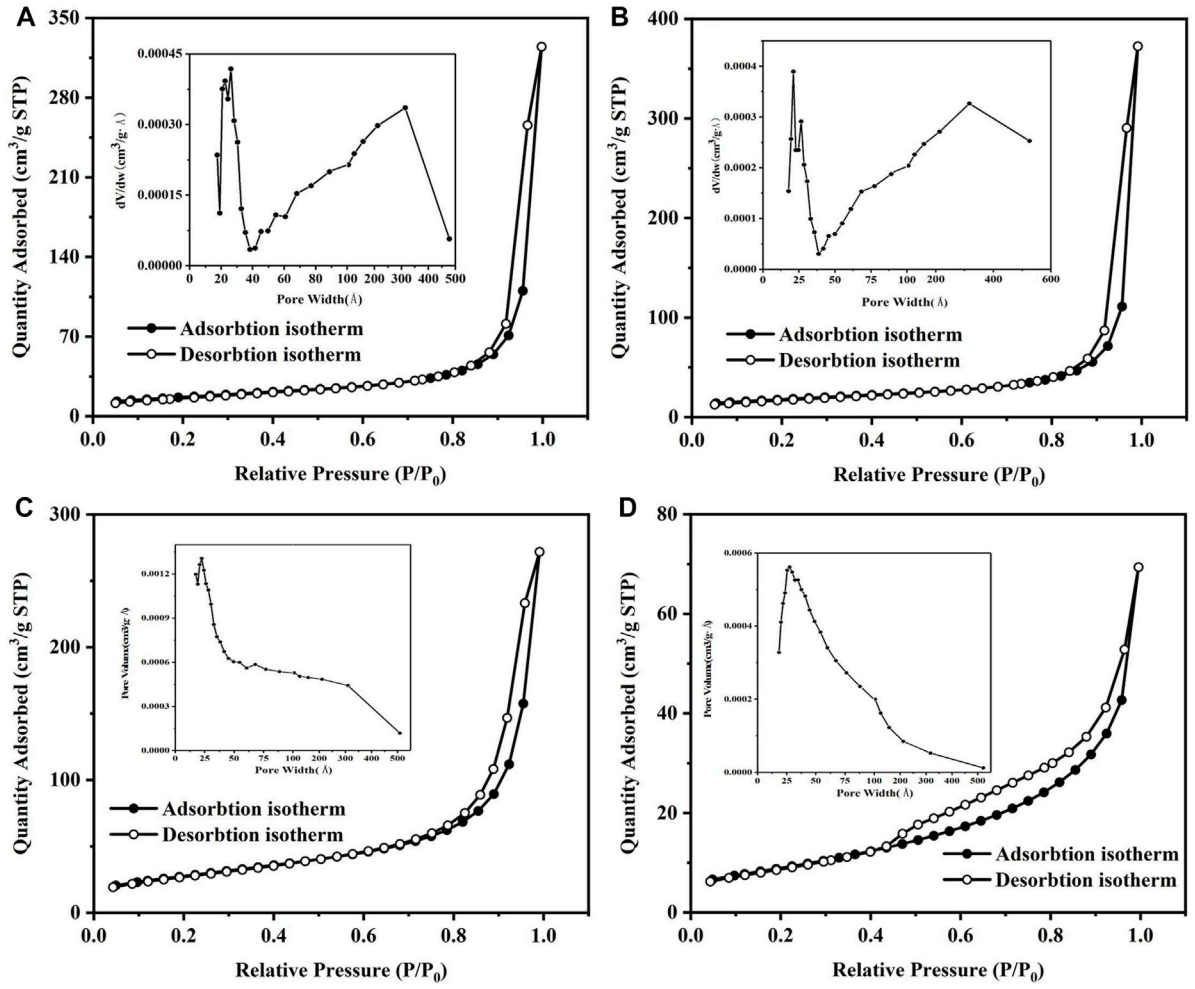

FIGURE 4
N_2 adsorption and desorption curves of **(A)** pure goethite, **(B)** 5% Co, **(C)** 10% Co, and **(D)** 20% Co isomorphic substituted goethite.

TABLE 2 Specific surface area, pore volume, and pore size of goethite with different Co isomorphic substituted content.

Sample	SSA (m^2/g)	Volume of single point pore (cm^3/g)	Average pore size (Å)
Co-G-0	59.7397	0.502449	336.4258
Co-G-5	62.7441	0.576426	367.4770
Co-G-10	99.0865	0.420523	169.7600
Co-G-20	32.8098	0.107317	130.8358

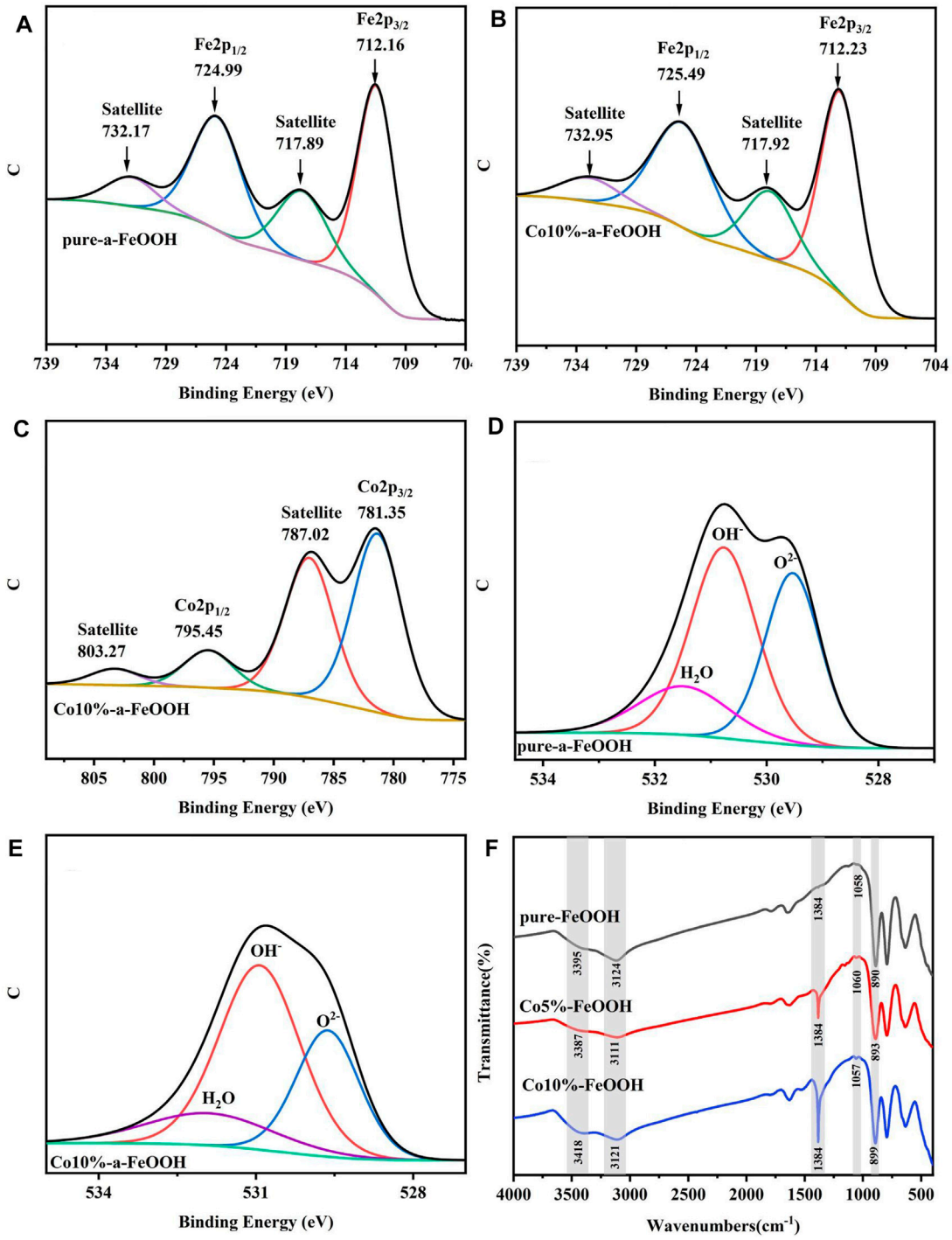

FIGURE 5
The narrow-line region spectra of Fe 2p **(A, B)**, Co 2p **(C)**, O 1s **(D, E)**, and the FT-IR spectra of samples **(F)**.

TABLE 3 Binding energies (eV) of Co 2p in different samples.

Samples	Co 2p 1/2	Co 2p 3/2	△B.E.	Ref.
CoOOH	795.30	780.20	15.10	Crowther et al. (1983)
$Co(OH)_2$	796.90	781.00	15.90	Crowther et al. (1983)
Co-G-10	795.45	781.25	14.20	This work

TABLE 4 The presence and proportion of oxygen on the surface before and after Co isomorphism substitution goethite.

Samples	B.E/eV	Surface species	Content (%)
Co-G-0	529.53	O^{2-}	36.03
	530.77	OH^-	47.22
	531.48	H_2O	16.75
Co-G-10	529.63	O^{2-}	29.70
	530.93	OH^-	55.70
	531.89	H_2O	15.23

2p, it can be seen from Figures 5A, B that there were two distinct peaks at 712.16 eV and 724.99 eV, which correspond to Fe 2p 3/2 and Fe 2p 1/2 in goethite, respectively. These results were consistent with the conclusion in a previous study (Yang et al., 2016). Furthermore, two satellite peaks corresponding to Fe^{3+} appeared at 717.89 eV and 732.17 eV, which were shifted to a higher binding energy after the isomorphous substitution (Figure 5B); the possible reason for this was that the Co ions were incorporated into the crystal structure of the goethite and the electrons from Co were accepted, thus exhibited a higher binding energy.

The Co 2p 3/2 and Co 2p 1/2 peaks at 781.25 eV and 795.45 eV can be clearly observed in Figure 5C. The binding energies of Co 2p in different samples are listed in Table 3, and the electron spin splitting value of goethite substituted by Co isomorphism was 14.2 eV, which was smaller than 15.1 eV in the Co(III)OOH sample. Therefore, it can be concluded that Co ions existed in the form of Co(III) in the goethite structure.

Figures 5D, E shows the O 1s photoelectron spectra of the samples. It can be clearly seen from the figure that it was not a symmetrical spectrum, indicating the oxygen on the sample surface was not in the form of a single lattice oxygen, but in the forms of hydroxyl and surface water molecules (Rakovan et al., 2015). Generally, the electronegativity of hydrogen is about 2.1, which is higher than 1.83 of iron. Therefore, when hydrogen atoms are combined with oxygen atoms, the electron cloud density around the oxygen atoms is much greater than that of oxygen atoms combined with iron atoms. Because of this characteristic, a higher binding energy was illustrated in the XPS spectrum, which was also a good explanation for the different binding energies of O^{2-}, OH^-, and H_2O in XPS, and the shear energy increased sequentially.

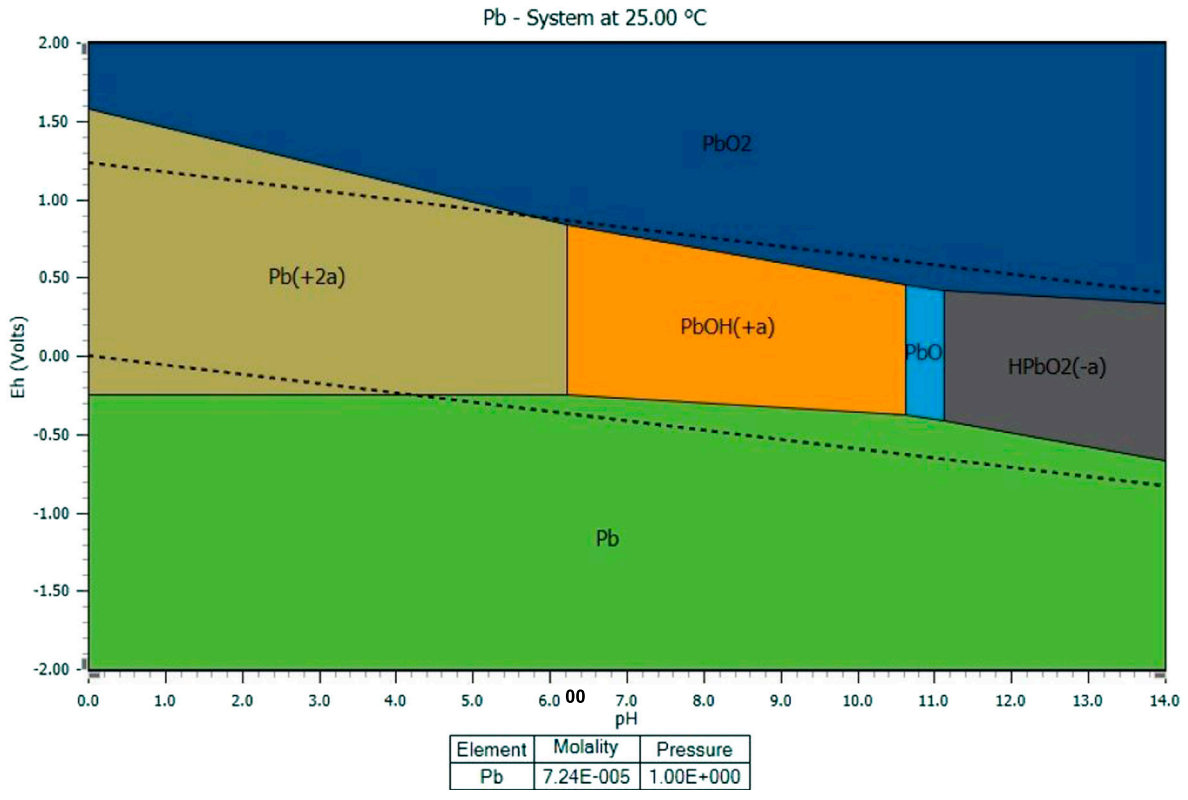

FIGURE 6
Eh-pH phase diagram of Pb-H_2O system.

TABLE 5 The cell parameters and energy band results calculated by DFT.

Content	0% (8Fe)	4.16% (1Co/23Fe)	12.5% (1Co/7Fe)	20. 8% (5Co/19Fe)
a(Å)	4.6388	4.5854	4.5869	4.5162
b(Å)	9.9845	9.9724	9.9622	9.9516
c(Å)	3.0356	3.0546	3.0100	2.9882
V (Å^3)	140.5971	139.6772	137.5438	134.2977
Band gap (eV)	1.229	1.024	0.856	0.829

The specific data is listed in Table 4. The peak positions of the chemical state were 529.53 eV and 529.63 eV, 530.77 eV and 530.93 eV, and 531.48 eV and 531.89 eV, corresponding to the O^{2-}, OH^-, and H_2O of the two samples, respectively. The results also showed that in the pure goethite, the three forms of O^{2-}, OH^-, and H_2O accounted for 36.03%, 47.22%, and 16.75%, while in the Co-substituted goethite, the proportions were 29.70%, 55.70%, and 15.23%, respectively. The hydroxyl on the surface of goethite increased due to the substitution of Co, which reduced the oxygen content of lattice oxygen and water molecules at the same time.

Figure 5F illustrates the FT-IR spectra of different samples. The peaks near 3,400 cm^{-1} and 3,120 cm^{-1} were assigned to -OH and -OH_2 and the peak at 1,384 cm^{-1} was generated by the bending vibration of -OH. Both the intensity of these peaks were increased with the increasing of Co content, especially the peak near 1,384 cm^{-1}, indicating that, as the content of Co increased, more hydroxyl groups were generated on the surface of goethite, and the O-H bending vibration amplitude was increased as well. Among the characteristic peaks of goethite, the peak at 1,057 cm^{-1} corresponded to the vibration of Fe-OH. From Figure 5F, it can be seen that the same enhancement trend as that of hydroxyl groups can be observed at 1,057 cm^{-1}. While there were no obvious enhancements observed of the peaks near 880 cm^{-1} (the peak positions of the 0%, 5%, and 10% samples were 890 cm^{-1}, 893 cm^{-1}, and 899 cm^{-1}, respectively), implying that the addition of Co exposed more Fe-OH groups on the surface of the goethite and had no significant impact on the internal structure of goethite (Fe-O-Fe).

3.2 DFT calculation

Density functional theory (DFT) calculations were performed in order to better study the effect of Co isomorphic substitution on the properties of goethite and Pb(II) removal from the atomic level. Due to the obvious intensity and high surface hydroxyl coverage, the (110) crystal plane was selected as the adsorption plane for study. The form of lead in water (30 mg/L), as shown in Figure 6, was calculated by HSC Chemistry software (Smith, 1996). Lead mainly exists in water as Pb^{2+} and $Pb(OH)^+$ at pH 6 and 7, respectively. Therefore, these two forms of lead were selected for DFT calculation.

3.2.1 Effect of cobalt isomorphic substitution on the properties of goethite

By modeling and optimizing the structure of goethite with different Co content, the calculated results are shown in Table 5, from which it can be seen that the values of cell parameters a, b, and c all decreased with the increasing of the amount of Co substitution and the unit cell volume was also reduced from 140.60 Å^3 to 133.27 Å^3. The DFT calculation results were consistent with those of the Rietveld refinement.

Energy band structure is an important parameter to describe the electrical conductivity of materials, and the band gap width can reflect the ability of electron transfer. The shorter the band gap, the stronger conductivity goethite has (Morgan, 2004). From Table 5, it can be seen that the band gap between the conduction band and the valence band became shorter, from 1.229 eV to 0.829 eV, which was due to the increasing of Co content. It was one of the reasons why the Co-substituted goethite had a stronger ability to adsorb Pb(II).

The total density of states was more biased towards the Fermi level in Co-substituted goethite, making the surface electrons more active. In addition, the partial density of states (PDOS) of O atoms in the samples were also investigated. It can be observed from Figure 7 that the PDOS of O atoms in the lattice of Co-substituted goethite was stronger than that of pure goethite. Since electrons were more active near the Fermi level than at other valence bands, the introduction of Co made the O atoms more electronegative. Another reason was that Co made the O atoms undergo less charge transfer during the bonding process. According to the Fukui function calculation (Table 6), the nucleophilic coefficient of the O connected to Co on the surface was larger, indicating that it had more advantages in cation adsorption.

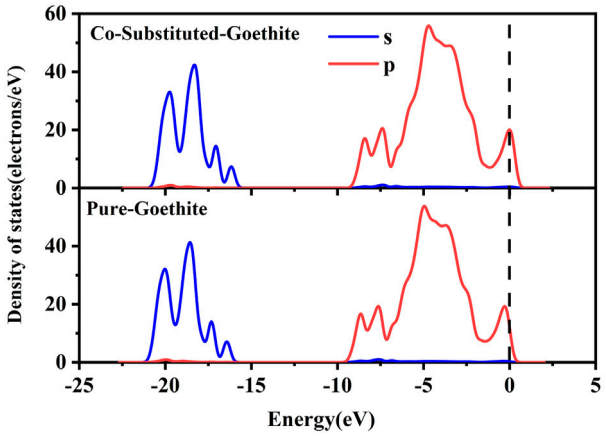

FIGURE 7
The PDOS of O before and after cobalt substitution.

TABLE 6 Electrophilic and nucleophilic coefficients of different O atoms on goethite surface.

Samples	Atom	Electrophilic coefficient (*f*-)	Nucleophilic coefficient (*f*+)
Pure goethite	O_a	0.002	0.002
	O_b	0.004	0.003
	O_c	0.012	0.012
Co-substituted goethite	O_a	0.002	0.007
	O_b	0.003	0.005
	O_c	0.011	0.012

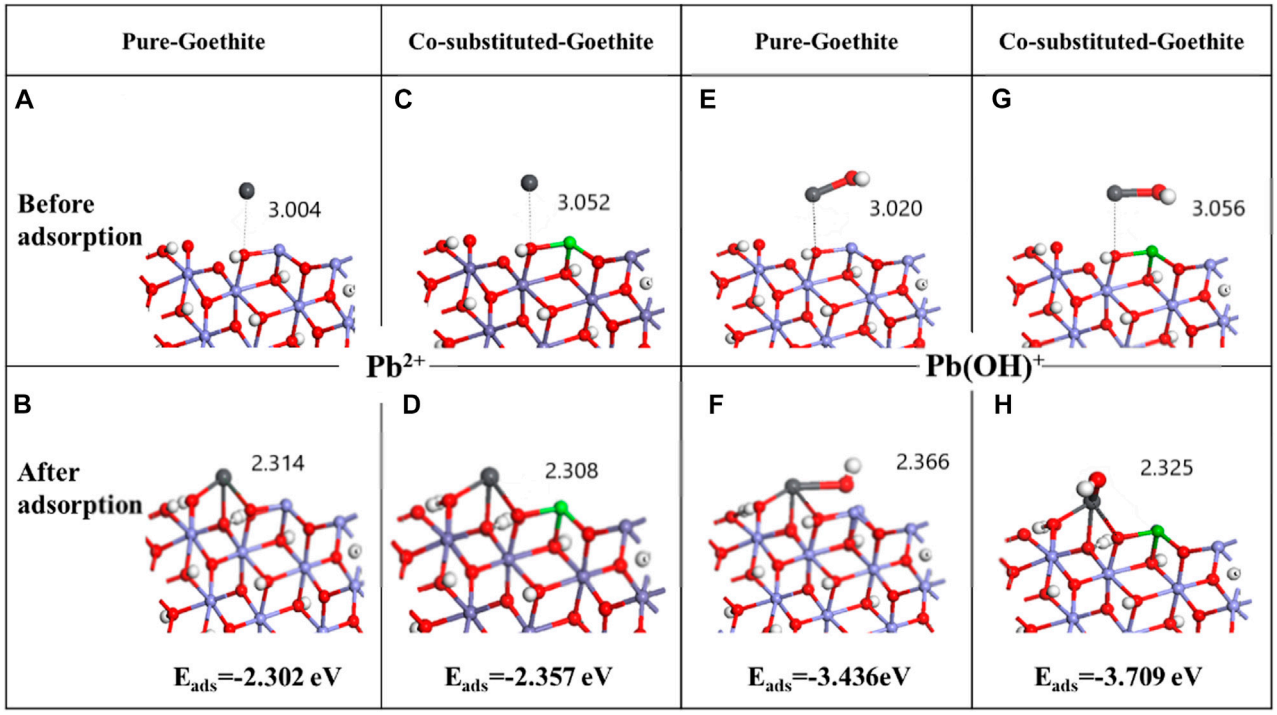

FIGURE 8
Configuration on the (110) plane of goethite before and after adsorption of Pb^{2+} **(A–D)** and $Pb(OH)^+$ **(E–H)**.

3.2.2 The adsorption of Pb^{2+} and $Pb(OH)^+$ on Co-substituted goethite

Figure 8 depicts the optimized configuration before and after the adsorption of Pb. Among them, Figures 8A–D are the configurations of pure goethite and Co-substituted goethite before and after the adsorption of Pb^{2+}, while Figures 8E–H are that of the adsorption of $Pb(OH)^+$. From these, it can be seen that both the Pb^{2+} and $Pb(OH)^+$ was adsorbed by goethite through the interaction with three surface hydroxyl groups and formed a tridentate complex with three oxygen atoms. The adsorption energy (E_{ads}) of the process of Pb^{2+} interaction with pure goethite and Co-substituted goethite were −2.302 eV (Figure 8B) and −2.357 eV (Figure 8D), respectively, indicating that there was a spontaneous exothermic reaction between lead and adsorbent. Moreover, the E_{ads} decreased from −2.302 to −2.357 after Co atom was doped, which illustrated that the interaction between Pb^{2+} and goethite was facilitated by Co and the adsorption product was more stable. The results of the adsorption of $Pb(OH)^+$ by goethite were similar to that of Pb^{2+}, but the E_{ads} of $Pb(OH)^+$ interacting with pure goethite and Co-substituted goethite were −3.436 eV and −3.709 eV, respectively, which were lower than that of Pb^{2+}, indicating that $Pb(OH)^+$ was easier to combine with goethite. Therefore, the results suggested that the Co atom acted as an active species, reducing the adsorption energy of the interaction process, which made lead more favorably adsorbed.

Figure 9 shows the partial density of states (PDOS) of O atoms and Pb atoms before and after the adsorption of Pb^{2+} by pure goethite and Co-substituted goethite. The O 2s orbital had three connected peaks at −17.0 to −21.0 eV, while the Pb 6p orbital had a weaker peak, indicating that the O 2s orbital resonated with the Pb 6p orbital within this range, forming a conventional sp3 hybridization and a bonding molecular orbital effect. In the

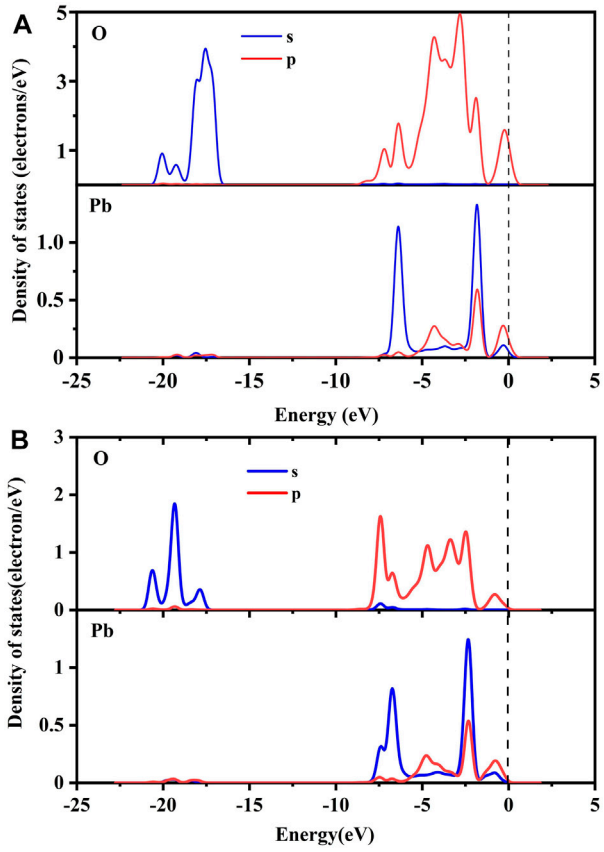

FIGURE 9
PDOS of pure goethite **(A)** and Co-substituted goethite **(B)** before and after adsorption of Pb^{2+}.

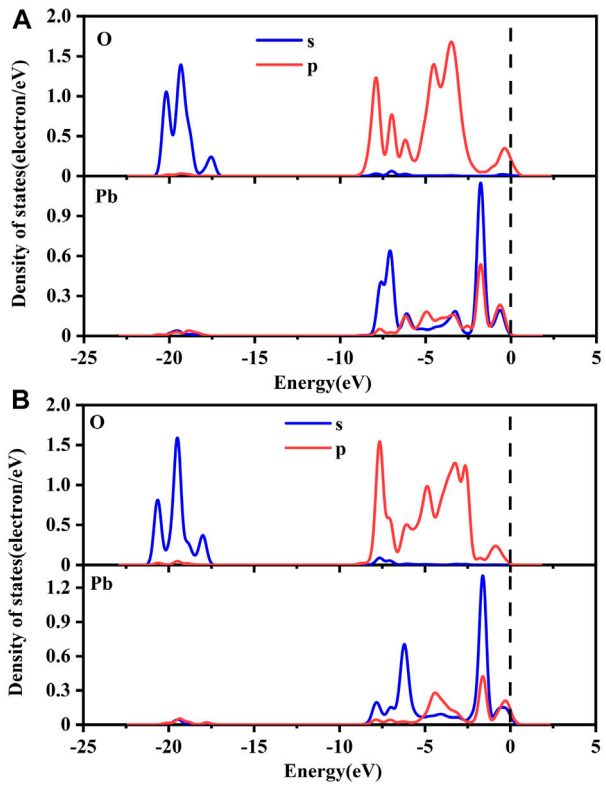

FIGURE 10
PDOS of pure goethite **(A)** and Co-substituted goethite **(B)** before and after adsorption of $Pb(OH)^+$.

range of −6.2 eV to −2.0 eV, the 6s and 6p orbitals of Pb coincided. Due to the large difference of the energy levels between the Pb 6s and 6p orbitals, it was difficult to form a conventional hybridization (He et al., 2023). At the same time, sharp peaks appeared because the energy levels of the Pb 6s and O 2p orbitals were relatively close, indicating that sp3 hybridization occurred between Pb 6s and O 2p and formed the role of an anti-bonding molecular orbital in the range of −6.2 eV to −2.0 eV. This also proved that Pb was adsorbed on the surface of goethite chemically, which was consistent with the previous analysis. Moreover, after the adsorption of Pb, the density of O at the Fermi level in p orbital was significantly lower than that of before adsorption, which implied that the adsorption of Pb reduced the reactivity of O and made the structure more stable than before.

The PDOS of O atoms and Pb atoms after adsorption of $Pb(OH)^+$ by pure goethite and Co-substituted goethite are shown in Figure 10. The DFT simulation results were similar to the adsorption of Pb^{2+} (Wang et al., 2015). In the range of −6.2 eV to −2.0 eV, Pb 6s and O 2p orbitals underwent a conventional sp3 hybridization, forming anti-bonding molecular orbitals. There was a weak peak in the 6p orbital of Pb in the range of −17.5 eV to −21.0 eV, which implied that the 2s orbital of O resonated with the 6p orbital of Pb in this range, forming a bonding molecular orbital effect.

4 Conclusion

The results in this study improve the understanding of the effect of Co-substituted goethite and the related sorption mechanisms of Pb(II). Cobalt existed in the form of Co(III) on the surface of goethite after substitution. The introduction of Co increased the degree of surface defects, with the unit cell parameters and volume of goethite decreasing with the increasing of Co content. Most importantly, it promoted the exposure of more hydroxyl groups (-OH) on the surface, which is the main functional group that reacts with Pb(II). The band gap width of goethite decreased, and the total density of states was more inclined to the Fermi level, making the surface electrons more active and the electron transfer efficiency higher. In addition, the analysis showed that the surface oxygen atoms connected to Co had a larger electronegativity, which was more advantageous for the adsorption of cations. These properties explain the mechanism of Co-substituted goethite to enhance lead adsorption. The adsorption equilibrium configuration displayed that both the Pb^{2+} and $Pb(OH)^+$ formed tridentate complexes with three oxygen atoms and this was a spontaneous exothermic reaction. The adsorption energy of Co-substituted goethite was higher and the adsorption equilibrium structure was more stable. Through the analysis of the density of states, it was found that the bonding mode of goethite in the adsorption of Pb was basically the same, all of which were sp3 hybridization. These adsorption mechanisms may help to better understand the changes in the

physiochemical properties of goethite and the adsorption process, highlighting the promotion of cobalt substitution in the adsorption and fixation of lead by goethite. The model parameters also help to expand the application of DFT calculations to the study of heavy metal ions adsorbed on soil minerals.

Data availability statement

The raw data supporting the conclusion of this article will be made available by the authors, without undue reservation.

Author contributions

XL: Methodology, software, formal analysis, investigation, and writing—original draft. WX: software, formal analysis, writing—original draft, and writing—review and editing. ZZ: writing—review and editing, data curation, and methodology. WZ: writing—review and editing. XH: conceptualization and supervision. SS: validation and supervision. MB: project administration. YL: methodology, validation, and investigation. All authors contributed to the article and approved the submitted version.

Funding

This work was financially supported by the National Natural Science Foundation of China (Grant Nos. 52074203, 32061123009), Qingchuang Talent Incubation Program from Colleges and universities in Shandong Province (Grant No. 2019.133).

Conflict of interest

The authors declare that the research was conducted in the absence of any commercial or financial relationships that could be construed as a potential conflict of interest.

The handling editor DL declared a shared affiliation with the author(s) XH at the time of review.

Publisher's note

References

Alvarez, M., Sileo, E. E., and Rueda, E. H. (2008). Structure and reactivity of synthetic Co-substituted goethites. *Am. Mineralogist* 93, 584–590. doi:10.2138/am.2008.2608

Cornell, R. M., Schwertmann, U., Gmbh, W. I. L., Kgaa, C., and Bern, U. (1996). The iron oxides. *Soil Mineralogy Environ. Appl.* 664, 363–369. doi:10.1002/3527602097

Crowther, D. L., Dillard, J. G., and Murray, J. W. (1983). The mechanisms of Co(II) oxidation on synthetic birnessite. *Geochimica Cosmochimica Acta* 47, 1399–1403. doi:10.1016/0016-7037(83)90298-3

Ding, N., Chen, X., and Wu, C. M. L. (2014). Interactions between polybrominated diphenyl ethers and graphene surface: A DFT and MD investigation. *Environ. Sci. Nano.* 1, 55–63. doi:10.1039/c3en00037k

Gasser, U. G., Jeanroy, E., Mustin, C., Barres, O., Nüesch, R., Berthelin, J., et al. (1996). Properties of synthetic goethites with Co for Fe substitution. *Clay Miner.* 31, 465–476. doi:10.1180/claymin.1996.031.4.03

He, F., Ma, B., Wang, C., Chen, Y., and Hu, X. (2023). Adsorption of Pb(II) and Cd(II) hydrates via inexpensive limonitic laterite: Adsorption characteristics and mechanisms. *Sep. Purif. Technol.* 310. doi:10.1016/j.seppur.2023.123234

Hsu, L.-C., Tzou, Y.-M., Ho, M.-S., Sivakumar, C., Cho, Y.-L., Li, W.-H., et al. (2020). Preferential phosphate sorption and Al substitution on goethite. *Environ. Sci. Nano.* 7, 3497–3508. doi:10.1039/c9en01435g

Huang, Y., Zhang, Z., Cao, Y., Han, G., Peng, W., Zhu, X., et al. (2020). Overview of cobalt resources and comprehensive analysis of cobalt recovery from zinc plant purification residue-a review. *Hydrometallurgy* 193. doi:10.1016/j.hydromet.2020.105327

HuanLiu, X., Lu, M. L. L., and Zhang, C., (2018). Structural incorporation of manganese into goethite and its enhancement of Pb(II) adsorption. *Environ. Sci. Technol.* 52. doi:10.1021/acs.est.7b05612

Hüffer, T., Sun, H., Kubicki, J. D., Hofmann, T., and Kah, M. (2017). Interactions between aromatic hydrocarbons and functionalized C 60 fullerenes–insights from experimental data and molecular modelling. *Environ. Sci. Nano.* 4, 1045–1053. doi:10.1039/c7en00139h

Ireta, J., Neugebauer, J., and Scheffler, M. (2004). On the accuracy of DFT for describing hydrogen bonds: Dependence on the bond directionality. *J. Phys. Chem. A* 108, 5692–5698. doi:10.1021/jp0377073

Iwasaki, K., and Yamamura, T. (2002). Whisker-like goethite nanoparticles containing cobalt synthesized in a wet process. *Mater. Trans.* 43, 2097–2103. doi:10.2320/matertrans.43.2097

Jackson, M. L. (2005). *Soil chemical analysis: Advanced course*. Madison, Wisconsin: UW-Madison Libraries Parallel Press.

Kubicki, J. D., Tunega, D., and Kraemer, S. (2017). A density functional theory investigation of oxalate and Fe(II) adsorption onto the (010) goethite surface with implications for ligand- and reduction-promoted dissolution. *Chem. Geol.* 464, 14–22. doi:10.1016/j.chemgeo.2016.08.010

Kühnel, R. (1975). The crystallinity of minerals—a new variable in pedogenetic processes: A study of goethite and associated silicates in laterites. *Clays Clay Minerals* 23, 349–354. doi:10.1346/ccmn.1975.0230503

Liang, Y., Yu, D., Jin, J., Xiong, J., Hou, J., Wang, M., et al. (2021). Microstructure of Al-substituted goethite and its adsorption performance for Pb(II) and As(V). *Sci. Total Environ.* 790. doi:10.1016/j.scitotenv.2021.148202

Liu, H., Chen, T., Zou, X., Qing, C., and Frost, R. L. (2013). Effect of Al content on the structure of Al-substituted goethite: A micro-Raman spectroscopic study. *J. Raman Spectrosc.* 44, 1609–1614. doi:10.1002/jrs.4376

Liu, Z., Peng, W., Xu, Z., Shih, K., Wang, J., Wang, Z., et al. (2016). Molybdenum disulfide-coated lithium vanadium fluorophosphate anode: Experiments and first-principles calculations. *ChemSusChem* 9, 2122–2128. doi:10.1002/cssc.201600370

Morgan, C. D. (2004). The electronic structure and band gap of LiFePO4 and LiMnPO4. *Solid State Commun.* 132. doi:10.1016/j.ssc.2004.07.055

Norrish, K. (1975). Geochemistry and mineralogy of trace elements. *Trace Elem. Soil-plant-animal Syst.* 55. doi:10.1016/B978-0-12-518150-1.50010-0

Rakovan, J., Becker, U., and Hochella, M. F. (2015). Aspects of goethite surface microtopography, structure, chemistry, and reactivity. *Am. Mineralogist* 84. doi:10.2138/am-1999-5-624

Schwertmann, U., and Fitzpatrick, R., (1977). Occurrence of lepidocrocite and its association with goethite in natal soils. *Soil Sci. Soc. Am. J.* 41, 1013–1018. doi:10.2136/sssaj1977.03615995004100050042x

Shannon, R. D. (1976). Revised effective ionic radii and systematic studies of interatomic distances in halides and chalcogenides. *Acta Crystallogr. Sect. A* 32, 751–767. doi:10.1107/s0567739476001551

Sileo, E. E., Ramos, A. Y., Magaz, G. E., and Blesa, M. A. (2004). Long-range vs. short-range ordering in synthetic Cr-substituted goethites. *Geochimica Cosmochimica Acta* 68, 3053–3063. doi:10.1016/j.gca.2004.01.017

Smith, W. R. (1996). HSC chemistry for windows, 2.0. *J. Chem. Inf. Model.* 36, 151–152. doi:10.1021/ci9503570

Song, W., Yang, T., Wang, X., Sun, Y., Ai, Y., Sheng, G., et al. (2016). Experimental and theoretical evidence for competitive interactions of tetracycline and sulfamethazine with reduced graphene oxides. *Environ. Sci. Nano.* 3, 1318–1326. doi:10.1039/c6en00306k

van Geen, A., Robertson, A. P., and Leckie, J. O. (1994). Complexation of carbonate species at the goethite surface: Implications for adsorption of metal ions in natural waters. *Geochimica Cosmochimica Acta* 58, 2073–2086. doi:10.1016/0016-7037(94)90286-0

Wang, J., Xia, S., and Yu, L. (2015). Adsorption of Pb(II) on the kaolinite(001) surface in aqueous system: A DFT approach. *Appl. Surf. Sci.* 339, 28–35. doi:10.1016/j.apsusc.2015.02.114

Yang, Z., Zhang, Z., Jiang, Y., Chi, M., Nie, G., Lu, X., et al. (2016). Palladium nanoparticles modified electrospun CoFe2O4 nanotubes with enhanced peroxidase-like activity for colorimetric detection of hydrogen peroxide. *RSC Adv.* 10, 33636–33642. doi:10.1039/c6ra01527a

Yi, H., Zhang, X., Jia, F., Wei, Z., Zhao, Y., and Song, S. (2019). Competition of Hg 2+ adsorption and surface oxidation on MoS 2 surface as affected by sulfur vacancy defects. *Appl. Surf. Sci.* 483, 521–528. doi:10.1016/j.apsusc.2019.03.350

Yu, N., Wang, L., Li, M., Sun, X., Hou, T., and Li, Y. (2015). Molybdenum disulfide as a highly efficient adsorbent for non-polar gases. *Phys. Chem. Chem. Phys. PCCP* 17, 11700–11704. doi:10.1039/c5cp00161g

Zhang, X., Zhang, L., Liu, Y., Li, M., Wu, X., Jiang, T., et al. (2020). Mn-Substituted goethite for uranium immobilization: A study of adsorption behavior and mechanisms. *Environ. Pollut.* 262, 114184. doi:10.1016/j.envpol.2020.114184